

VQ-HPS: HUMAN POSE AND SHAPE ESTIMATION IN A VECTOR-QUANTIZED LATENT SPACE

Guénolé Fiche¹, Simon Leglaive¹, Xavier Alameda-Pineda², Antonio Agudo³, and Francesc Moreno-Noguer³

¹CentraleSupélec, IETR UMR CNRS 6164, France

²Inria, Univ. Grenoble Alpes, CNRS, LJK, France

³Institut de Robòtica i Informàtica Industrial, CSIC-UPC, Barcelona, Spain

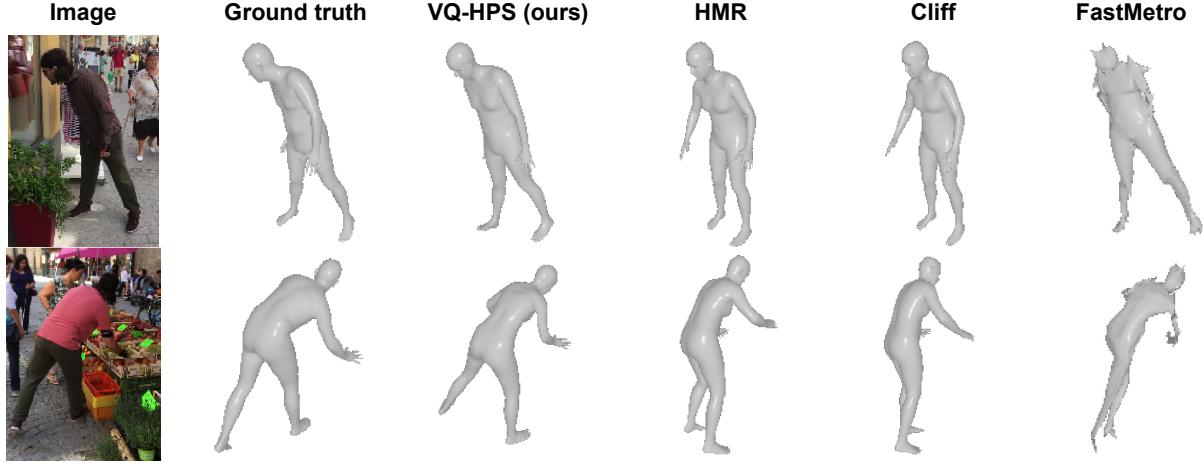


Figure 1: **VQ-HPS formulates the human pose and shape estimation problem as a classification task in a vector-quantized latent space.** We present the results of VQ-HPS on two challenging scenarios with in-the-wild conditions and poor illumination, comparing its performance to that of HMR [25], Cliff [36] and FastMETRO [7].

ABSTRACT

Human Pose and Shape Estimation (HPSE) from RGB images can be broadly categorized into two main groups: parametric and non-parametric approaches. Parametric techniques leverage a low-dimensional statistical body model for realistic results, whereas recent non-parametric methods achieve higher precision by directly regressing the 3D coordinates of the human body. Despite their strengths, both approaches face limitations: the parameters of statistical body models pose challenges as regression targets, and predicting 3D coordinates introduces computational complexities and issues related to smoothness.

In this work, we take a novel approach to address the HPSE problem. We introduce a unique method involving a low-dimensional discrete latent representation of the human mesh, framing HPSE as a classification task. Instead of predicting body model parameters or 3D vertex coordinates, our focus is on forecasting the proposed discrete latent representation, which can be decoded into a registered human mesh. This innovative paradigm offers two key advantages: firstly, predicting a low-dimensional discrete representation confines our predictions to the space of anthropomorphic poses and shapes; secondly, by framing the problem as a classification task, we can harness the discriminative power inherent in neural networks.

Our proposed model, VQ-HPS, a transformer-based architecture, forecasts the discrete latent representation of the mesh, trained through minimizing a cross-entropy loss. Our results demonstrate that VQ-HPS outperforms the current state-of-the-art non-parametric approaches while yielding results as

realistic as those produced by parametric methods. This highlights the significant potential of the classification approach for HPSE.

1 Introduction

Capturing and understanding human motion from RGB data is a fundamental task in computer vision, with many applications such as character animation for the movie and video-game industries [18, 58, 74] or performance optimization in sports [15, 65]. However, due to depth ambiguity, estimating 3D human pose and shape from monocular images is an underdetermined problem. To overcome this issue, parametric approaches (also called model-based) use statistical models of the human body, which enable the reconstruction of a human 3D mesh by predicting a small number of parameters [1, 40, 46, 48, 67]. Earlier methods were optimization-based, estimating the parameters of a human body model iteratively using 2D cues [4, 34, 49]. However, their need for a good initialization, slow running time, and propensity to converge towards local minima led many recent works to focus on regression-based methods, which predict the parameters of a human body model directly from RGB data [19, 25, 36]. Despite producing realistic results in most scenarios, methods regressing the parameters of a human body model face several issues well documented in the literature: 1) Parametric methods struggle in capturing detailed body shape and are biased towards the mean shape [12]; 2) Most human body models use rotations along the kinematic tree for expressing the pose. In addition to being difficult to predict for neural networks [9, 32], this representation induces error accumulation when all rotations are predicted simultaneously [64, 72]; 3) Most regression methods extract global feature vectors from the image as an input, which do not contain fine-grained local details [39].

In order to alleviate these issues, several works switched to methods inspired by 3D pose estimation models that predict 3D coordinates directly. Earlier methods predicted the 6890 vertices of the full SMPL [40] mesh using graph convolutional neural networks (GCNNs) modeling the mesh structure and focusing on local interaction between neighboring vertices [9, 32]. While [38] used Transformers [62] to model global interactions between joints and vertices, others argued that a hybrid architecture mixing GCNNs and Transformers would enable modeling both local and global interactions [39]. More recently, FastMETRO [7] proposed a transformer-based encoder-decoder architecture to disentangle image and mesh features and predicted 3D coordinates of body joints and a coarse mesh that can be upsampled to the full SMPL body mesh. Significantly different from prior works, LVD [12] proposed an optimization-based approach estimating each vertex position independently by predicting vertex displacement with neural fields. Despite proposing alternatives to model-based approaches, these methods also present some drawbacks: 1) Approaches regressing all vertices of the body mesh at once lack global interaction modeling when using GCNNs [39] and have a very high computational cost when using Transformers [7, 14]; 2) Regression-based methods sometimes output noisy meshes, some of them regress the SMPL parameters from the predicted mesh to obtain smoother predictions, but it comes with a loss of accuracy [7, 9, 32]; 3) LVD [12] is real-time and obtains state-of-the-art results for shape estimation, but is not adapted to extreme poses.

This work introduces a method significantly different from all prior human pose and shape estimation approaches. Instead of predicting the parameters of a human body model or 3D coordinates, we learn to predict a discrete latent representation of 3D meshes, transforming the HPSE into a classification problem, in which we can exploit the discriminative power of transformers. Concretely, for learning our discrete latent representation of meshes, we build on the vector quantized-variational autoencoder (VQ-VAE) [60] framework and adapt it to the fully convolutional mesh autoencoder proposed in [78]. The encoder of the proposed model, called Mesh-VQ-VAE, provides a low-dimensional discrete latent representation preserving the spatial structure of the mesh. We then propose a transformer-based encoder-decoder model, called VQ-HPS, for learning to solve the HPSE problem using the cross-entropy loss. Once the mesh discrete representation is predicted, we can decode it using the Mesh-VQ-VAE decoder and obtain a full mesh following the SMPL mesh topology [40]. Since the Mesh-VQ-VAE is learned on a large human motion capture database [43], it automatically learns to decode smooth and realistic human meshes.

VQ-HPS achieves state-of-the-art performance on the challenging 3DPW [63] benchmark. It outperforms other methods quantitatively while producing qualitative results as realistic as parametric methods (see Fig. 1).

Our key contributions can be summarized as follows:

- A Mesh-VQ-VAE architecture providing a discrete latent representation of 3D meshes.
- A classification-based formulation of the HPSE problem using the introduced discrete latent representation of human meshes.
- VQ-HPS, a transformer-based encoder-decoder model learning to solve the proposed HPSE classification problem using the cross-entropy loss.

2 Related Work

2.1 Parametric Approaches

Several methods are dedicated to recovering the parameters of a parametric human model, such as SMPL [40]. Optimization techniques iteratively estimate the parameters of a body model based on images or videos, ensuring that the projection of predictions aligns with a set of 2D cues, including 2D skeletons [4, 16, 24, 48], part segmentation [34, 71], or DensePose [20]. Pose and motion priors are commonly incorporated into optimization methods to enhance the realism of predictions [42, 49, 56, 59]. On the contrary, regression methods employ neural networks to predict the parameters of a human body model from input images or videos. Many of these methods leverage convolutional neural networks (CNNs) for extracting image features [8, 25, 26, 29–31, 36, 68, 69, 73]. Recent works have demonstrated remarkable performance by replacing CNNs with Vision Transformers [13] as seen in [5, 19, 37, 76]. Some methods output probabilistic results, enabling sampling among plausible solutions [2, 17, 33, 54, 55]. While optimization methods typically yield superior results, they come with significantly longer running times than regression methods and require precise initialization and accurate 2D cues. One limitation in training regression models lies in the scarcity of datasets containing RGB data with 3D annotations. Prior works have addressed this challenge by employing synthetic data [3, 6, 47, 54, 61] or pseudo-labels [24, 34, 44] for training their models.

While parametric models offer the capability to estimate reasonable human poses, the model parameter space may not be the most suitable focus for predicting human pose and shape [12, 32]. Recognizing these limitations inherent in parametric approaches has spurred the development of non-parametric methods.

2.2 Non-parametric Approaches

Several works have explored methods for directly predicting 3D meshes without relying on the parameters of a human body model [7, 12, 32, 38, 39, 45]. In earlier approaches, regression architectures based on Graph Convolutional Neural Networks (GCNNs) were proposed, utilizing a graph structure derived from the topology of the SMPL human mesh [32, 39, 45]. Recent advancements have leveraged Transformer architectures, capitalizing on attention mechanisms to capture relationships between joints and vertices. While approaches like [38, 39] have introduced encoder-based strategies that concatenate image features and mesh tokens for predicting 3D coordinates, FastMETRO [7] presented an encoder-decoder architecture, effectively disentangling image and mesh modalities. Recently, [14] introduced a token pruning strategy to enhance the efficiency of transformer-based HPSE, and [12] achieved state-of-the-art accuracy in body shape estimation through an optimization-based approach relying on per-vertex neural features.

In this work, we introduce a non-parametric approach to Human Pose and Shape Estimation (HPSE). Our objective is to estimate the vertices of a human body mesh, adhering to the SMPL topology [40]. In contrast to all prior works, our method involves predicting the mesh through a discrete latent representation, reframing HPSE as a classification problem. Although exploiting the discriminative power of classification networks has already been proposed for the Human Pose Estimation (HPE) problem (see below), to the best of our knowledge, this has not been done before for the HPSE problem.

2.3 Quantization of the Human Pose and Shape

A number of works explored the use of quantization for Human Pose Estimation (HPE). [35] proposed to discretize horizontal and vertical coordinates for 2D HPE. On the other hand, [50, 51] used anchor poses and refined them for solving the 3D HPE problem. [11] proposed a human pose and shape classification method, but the system was trained on only 12 different postures. Some approaches proposed hand shape classification [28], especially for sign-language recognition following the works of [10]. Some works also proposed face shape classification [53] and head pose estimation [21] using a Support Vector Machine.

Similar to ours, recent works in human motion generation [41, 57, 70, 75] used a VQ-VAE [60] for quantizing human motion. The main difference between these models and Mesh-VQ-VAE is that in these works, a single index encodes a sequence of poses, whereas we use several indices to encode a single pose, allowing for higher precision. Also, none of these works encode the 3D mesh: [41] works on the SMPL parameters, and others only encode a 3D skeleton.

3 Background

SMPL model. SMPL [40] is a skinned vertex-based model that maps the body shape parameter $\beta \in \mathbb{R}^{10}$ and the pose parameter $\theta \in \mathbb{R}^{72}$ to 3D vertices through the differentiable function $\mathcal{M}(\beta, \theta)$. It outputs the 3D vertices $V \in \mathbb{R}^{6890 \times 3}$ of a registered mesh, and 3D joints $J \in \mathbb{R}^{24 \times 3}$ can be extracted from the mesh using the joint regressor matrix \mathcal{J}_{smpl} .

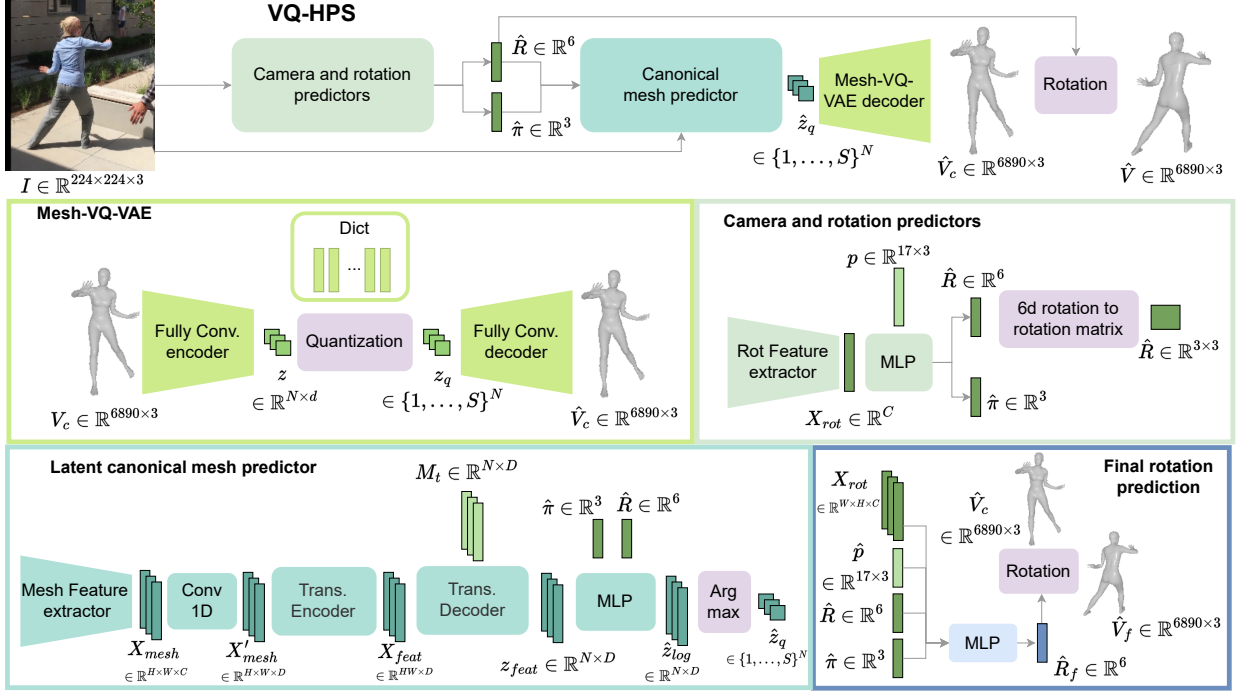


Figure 2: **VQ-HPS global process for predicting the mesh given an image.** The first step is to predict the camera $\hat{\pi}$ and the rotation \hat{R} from the image I . Then, we use the image, the predicted rotation, and the camera to predict the vertices \hat{V}_c of the canonical mesh. Finally, \hat{V}_c is rotated according to \hat{R} to obtain the final mesh vertices \hat{V} . Details about the architecture of VQ-HPS components are also given.

In this work, we do not predict the parameters of the SMPL model, as prior works [9, 12, 32] showed that they are not a suitable target for regression models. However, the mesh predicted by the proposed VQ-HPS model follows the SMPL mesh topology. It allows us to use tools like joint regressors and provides a fair comparison with existing approaches.

Fully convolutional mesh autoencoder. The fully convolutional mesh autoencoder [78] is an autoencoder specifically tailored for handling arbitrary registered mesh data. It relies on the definition of novel convolution and pooling operators with globally shared weights and locally varying coefficients depending on the mesh structure. These variable coefficients play a pivotal role in capturing intricate details inherent to irregular mesh connections, contributing to the model’s exceptional performance in mesh reconstruction. One of the main advantages of the fully convolutional architecture is that the latent codes are localized, which gives a latent space preserving the spatial structure of the mesh. The latent representation of the fully convolutional mesh autoencoder lies in $\mathbb{R}^{N \times d}$ where N is the number of latent vectors, and d is the dimension of latent vectors.

Vector quantized-variational autoencoder. The VQ-VAE [60] is an encoder-decoder model with a discretized latent space. The idea is to learn jointly an encoder, a dictionary of latent codes, and a decoder. The encoder maps the input data x into a latent variable $z \in \mathbb{R}^{N \times d}$. We then discretize z using a learned dictionary of S latent codes. We can then write $z_d \in \mathbb{R}^{N \times d}$ where each vector of z is replaced by the closest latent code, or $z_q \in \{1, \dots, S\}^N$, where the index of the closest latent code replaces each vector of z . The decoder reconstructs x from the discrete latent representation z_d and the learned dictionary.

4 Method

4.1 Proposed HPSE method

We propose a novel classification-based method for HPSE. Our goal is to predict an oriented 3D mesh from an image. VQ-HPS consists of an encoder-decoder architecture, predicting the human mesh discrete representation of the introduced Mesh-VQ-VAE from image features. We believe that this is the most adapted architecture for predicting our discrete latent representation, with encoder tokens corresponding to image patches and the decoder tokens corresponding to parts of the body and indices in the latent space. In order to ease the low-dimensional representation learning of

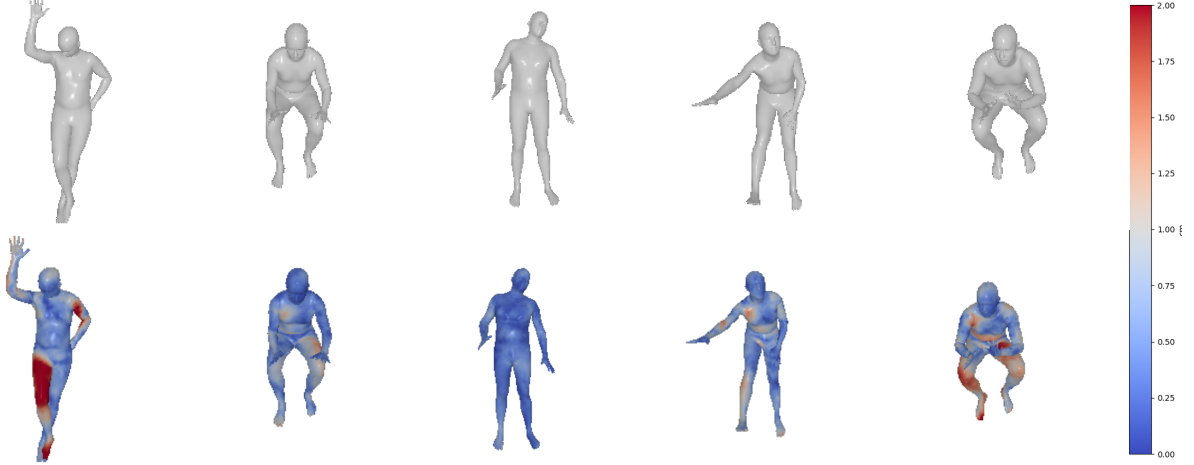


Figure 3: figure

Mesh-VQ-VAE reconstruction error. Samples of reconstruction on the 3DPW test set. The error is in cm and corresponds to the Euclidean distance between the original mesh and the corresponding vertex in the reconstruction.

the mesh, the predicted mesh is non-oriented and centered on the origin (see Sec. 4.2): we call it a *canonical mesh*. To obtain the final oriented mesh, we then need to predict the rotation $R \in \mathbb{R}^{3 \times 3}$, and for better alignment with the image, we also regress the perspective camera $\pi = [s, t] \in \mathbb{R}^3$ where s is a scale parameter and t is a 2D translation. The overall method is shown in Fig. 2, and we will now proceed to detail each of its primary components.

Mesh-VQ-VAE. For learning discrete representations of meshes, we build on the fully convolutional mesh autoencoder [78] (see Sec. 3) for encoding the full mesh vertices $V \in \mathbb{R}^{6890 \times 3}$ to a latent representation $z \in \mathbb{R}^{N \times d}$. We add a quantization step in the latent space similar to [60] (see Sec. 3). z is mapped to the discrete latent representation $z_q \in \{1, \dots, S\}^N$. While the fully convolutional architecture preserves the spatial structure of the mesh, the added quantization step allows us to view the HPSE as a classification task. Our Mesh-VQ-VAE Fig. 2 can be seen as a VQ-VAE [60] where the encoder and decoder networks are the fully convolutional mesh autoencoder.

Feature extractors. The first step for image-based HPSE is to extract features from the image. We use CNN backbones to preserve the spatial structure of the image, and we obtain features $X \in \mathbb{R}^{H \times W \times C}$, where C is the number of channels of the backbone and $H \times W$ is the spatial dimension size. We use two backbones: one for predicting the global rotation and another for the pose and shape prediction.

Rotation and camera prediction. We start by predicting the mesh rotation and the perspective camera parameters (see again Fig. 2). These predictions depend on the image features and on an initial body pose $p \in \mathbb{R}^{17 \times 3}$ following the Human3.6M [23] joints layout. We predict the rotation \hat{R} and the weak perspective camera parameters $\hat{\pi}$.

Latent canonical mesh regressor encoder. The transformer encoder inputs are the features extracted by the CNN backbone. Before being fed to the Transformer encoder, we apply a 1D-convolution on the image features to make them of dimension $X'_{mesh} \in \mathbb{R}^{H \times W \times D}$ where D is the hidden state size of the Transformer. These features are flattened to obtain HW tokens of dimension D , and then we add positional encoding. The obtained tokens are fed to a Transformer encoder, using self-attention between all image tokens to output encoded image features $X_{feat} \in \mathbb{R}^{HW \times D}$.

Latent canonical mesh regressor decoder. The transformer decoder takes as inputs N learned mesh tokens M_i of size D , each responsible for predicting a dimension of the Mesh-VQ-VAE discrete latent representation. The Transformer decoder consists of self-attention between learned tokens and cross-attention with image features. It outputs latent mesh features $z_{feat} \in \mathbb{R}^{N \times D}$. Then (see Fig. 2), to obtain the logits $\hat{z}_{log} \in \mathbb{R}^{N \times S}$, we rely on the mesh features as well as on the previously predicted rotation and camera. We obtain the predicted discrete representation $\hat{z}_q \in \{1, \dots, S\}^N$ by applying an $\arg \max(\cdot)$ operation.

Reconstructing the full mesh. From the mesh discrete latent representation $\hat{z}_q \in \{1, \dots, S\}^N$, we use the decoder of the introduced Mesh-VQ-VAE to reconstruct the vertices of a full canonical mesh $\hat{V}_c \in \mathbb{R}^{6890 \times 3}$. To obtain the vertices \hat{V} of the oriented mesh in the frame coordinates, we apply the predicted rotation \hat{R} to the vertices. This process is shown in Fig. 2.

4.2 Implementation details

Mesh-VQ-VAE. The Mesh-VQ-VAE architecture (see Fig. 2) is adapted from the fully convolutional mesh autoencoder of [78]. This model encodes a mesh to a latent representation $z \in \mathbb{R}^{N \times d}$ with $N = 54$ and $d = 9$. The quantization step is performed with a dictionary of size $S = 512$.

Feature extractors. In order to provide a fair comparison with previous methods, our CNN backbones are ResNet-50 [22] pre-trained on ImageNet [52]. For the canonical mesh prediction, we remove the last fully connected layer to obtain features $X_{mesh} \in \mathbb{R}^{H \times W \times C}$ with $H = W = 7$, $C = 2048$. For the rotation and camera prediction, we keep the full Resnet-50 to obtain features $X_{rot} \in \mathbb{R}^C$.

Rotation and camera predictors. Inspired by [25], the network for predicting the rotation and the mesh consists of a multilayer perceptron (MLP) regression module composed of two fully connected layers with 1024 neurons following the CNN backbone (see Fig. 2). The image feature $X_{rot} \in \mathbb{R}^C$ is concatenated with the flattened pose $p \in \mathbb{R}^{17 \times 3}$ before being fed to the MLP. The rotation is predicted in the 6d-rotation format [77], and p is initialized with the SMPL T-pose.

Latent canonical mesh regressor. The Transformer’s hidden dimension is $D = 512$, and all multi-layer-perceptrons in the encoder and decoder have a hidden size of 1024. We use sinusoidal positional encoding for the input tokens.

4.3 Training VQ-HPS

VQ-HPS is trained in a supervised manner, given a dataset of RGB images paired with meshes. The canonical mesh predictor is trained solely on the discrete latent representation of meshes. For obtaining the latent representation of the ground truth and for decoding the predicted indices to a full mesh, we use the Mesh-VQ-VAE, which is pre-trained and frozen during the VQ-HPS training.

Mesh-VQ-VAE. The Mesh-VQ-VAE (see Fig. 2) is trained on the AMASS [43] dataset and finetuned on the 3DPW [63] training set. In order to ease the learning of the mesh discrete representation with a limited number of indices, we train the Mesh-VQ-VAE with non-oriented meshes translated to the origin (canonical meshes). The final reconstruction error is 4.7mm. This reconstruction error is an important parameter as it corresponds to the minimal per-vertex error (see Sec. 5.2) we can obtain. Qualitative results of reconstruction on 3DPW are shown in Fig. 3.

Latent canonical meshes. For learning to predict the pose and shape, we only use the discrete representation of the canonical mesh as the training target. The loss is the cross-entropy between the discrete latent representation of the ground truth mesh and the prediction:

$$\mathcal{L}_{mesh} = \text{Cross-entropy}(\hat{z}_{log}, z_q), \quad (1)$$

where \hat{z}_{log} are the predicted logits, and z_q is the discrete latent representation of the ground truth mesh.

Mesh rotation. We learn to predict the global orientation by computing a mean squared error between the ground truth and predicted rotation matrices:

$$\mathcal{L}_{rot} = \|\hat{R} - R\|_2, \quad (2)$$

where \hat{R} and R are the predicted and ground truth rotation matrices.

Reprojection. To guide the rotation learning and for better image alignment, we add a reprojection error. It is computed between the 2D projection (using the predicted weak-perspective camera) of the 3D joints extracted from the predicted mesh and the 2D ground truth joints. This loss is computed using the SMPL 24 joints, which can be extracted from the full mesh using a joint regressor \mathcal{J}_{smpl} (see Sec. 3). The reprojection loss is computed as:

$$\mathcal{L}_{2D} = \|\hat{s}\Pi(\hat{J}_{3D}) + \hat{t} - J_{2D}\|_1, \quad (3)$$

where \hat{s} is the predicted scale, \hat{t} the predicted 2D translation and \hat{J}_{3D} are the 3D joints computed from the predicted oriented mesh vertices $\hat{\mathcal{V}}$. Π is the orthographic projection using the matrix $\begin{bmatrix} 1 & 0 & 0 \\ 0 & 1 & 0 \end{bmatrix}^\top$ and J_{2D} are the ground truth 2D joints.

Learning scheme. The rotation prediction is learned using \mathcal{L}_{rot} and \mathcal{L}_{2D} . We use \mathcal{L}_{2D} for the camera and \mathcal{L}_{mesh} for the canonical mesh. \mathcal{L}_{2D} might help to learn the pose, but we chose not to use it to demonstrate that the cross-entropy is sufficient for making accurate predictions.

In order to improve the final prediction, we propose to add a final rotation predictor network (VQ-HPS-rot). This network takes as input the rotation image features X_{rot} , the predicted rotation \hat{R} , the predicted camera $\hat{\pi}$, and the

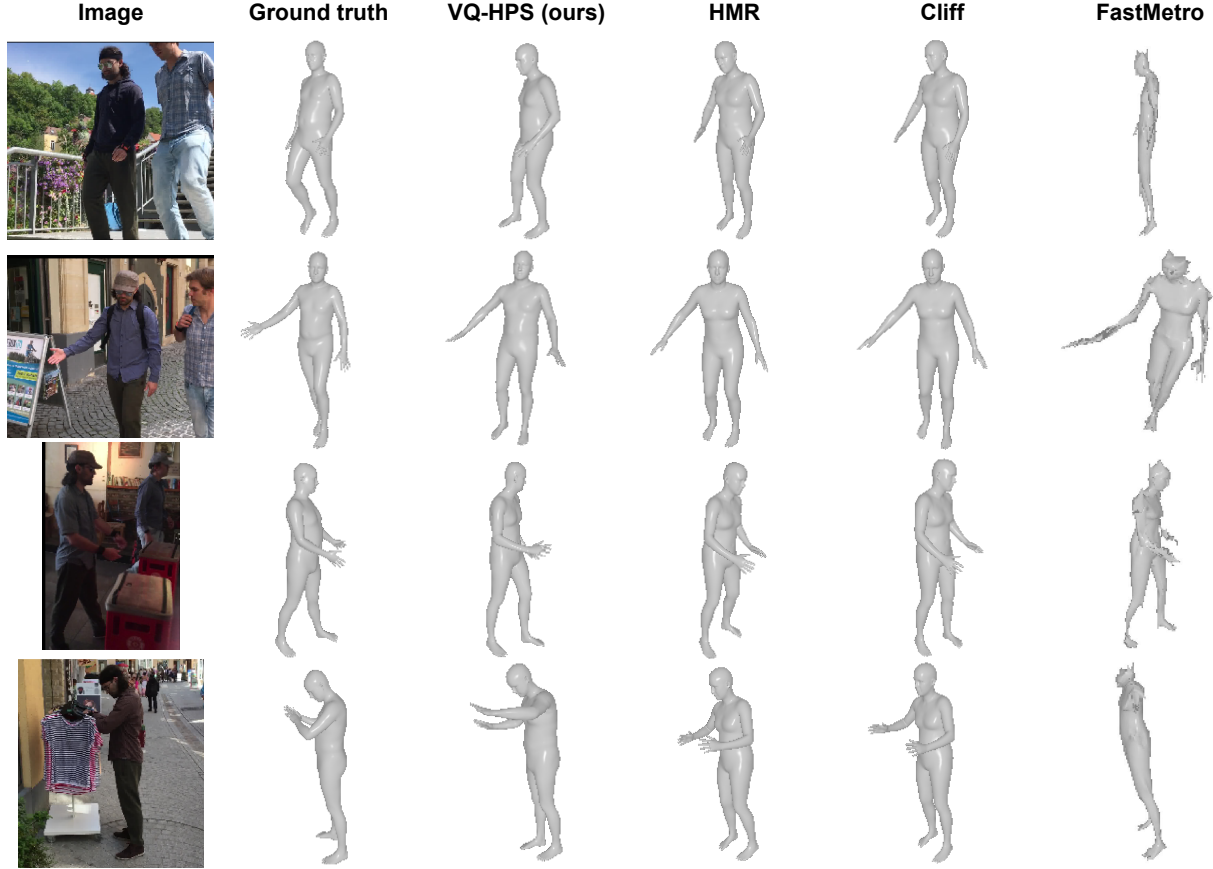


Figure 4: **Qualitative results** We compare our method with HMR [25], Cliff [36] and FastMetro [7].

predicted skeleton \hat{p} extracted from the predicted mesh \hat{V} using a joints extractor. It outputs a final rotation \hat{R}_f , which can be applied to the predicted canonical mesh \hat{V}_c to predict the final mesh \hat{V}_f . Fig. 2 overviews this process.

5 Results

5.1 Datasets

AMASS. The Mesh-VQ-VAE is trained on AMASS [43], which is a large database of human motion in the SMPL [40] format. It contains more than 11000 motions and 300 subjects, which makes it representative of the variety of body poses and shapes.

3DPW. This dataset [63] consists of 60 in-the-wild RGB videos with 3D ground truth for human bodies. We use the pre-defined splits for training, validation, and testing.

5.2 Metrics

We use several metrics for evaluating the predictions of VQ-HPS. All of them will be expressed in *mm* for the whole results section.

Per-vertex error (PVE) measures the Euclidean distance between the predicted vertices and the ground truth.

Mean-per-joint error (MPJPE) measures the Euclidean distance between the predicted joints and the ground truth. In our case, the joints are extracted from the predicted mesh using a joint regressor similar to \mathcal{J}_{smpl} .

Method	PVE ↓	MPJPE ↓	PA-MPJPE ↓
HMR [25]	209.34	177.57	89.31
Cliff [36]	223.90	188.82	<u>89.20</u>
FastMetro [7]	176.34	156.99	104.64
VQ-HPS (ours) ¹	<u>163.88</u>	<u>139.80</u>	84.92
VQ-HPS-rot (ours) ²	160.68	136.58	84.92

Table 1: **Quantitative results on 3DPW.** We compare VQ-HPS with SOTA methods using standard metrics.

Procrustes-aligned mean-per-joint error (PA-MPJPE) measures the Euclidean distance between the predicted joints and the ground truth after a Procrustes alignment.

5.3 Comparison to other methods

We train VQ-HPS on the 3DPW training set to see how it performs when trained on limited data. We compare our performance with HMR [25], Cliff [36], and FastMetro [7]. We chose these 3 models for comparison because HMR is the basic architecture for parametric human mesh recovery, Cliff is the state-of-the-art (SOTA) for parametric HPSE, and FastMetro is the SOTA for non-parametric HPSE and the closest method to ours. For this experiment, the backbone for all networks is ResNet-50 [22] pre-trained on ImageNet [52]. We use this backbone because it is the most used in the literature, and its small size seems an appropriate choice for training with limited data. We use the public implementation of FastMetro, and we adapt the implementations of HMR and Cliff provided by [3]. Quantitative results are shown in Tab. 1, and visualizations are available in Fig. 4. In Tab. 1, VQ-HPS denotes our model without the final rotation predictor presented in Sec. 4.3, while VQ-HPS-rot features this improved rotation prediction.

VQ-HPS achieves state-of-the-art results for MPJPE and PA-MPJPE while being very close to the best results in terms of PVE (see Tab. 1). While HMR and Cliff show lower performance in terms of PVE and MPJPE, FastMetro is not state-of-the-art in terms of PA-MPJPE. Our method is the only one showing good performance for all metrics. Visualization of the results confirms that our method performs best. Despite good metrics, FastMetro produces unsmooth results that do not correspond to human shapes. However, we should note that this is probably due to the limited training set, as the results displayed in the original paper looked realistic. This could also be due to the choice of the backbone, since results shown in [7] were obtained with the biggest version of the model, using HRNet-64 [66].

5.4 Ablation study

We ablate VQ-HPS architecture and training scheme and present the results in Tab. 2.

The ablation “3D loss” replaces the cross-entropy loss with the PVE $\mathcal{L}_{3D} = ||V - \hat{V}||_2$ where V is the ground truth mesh vertices and \hat{V} the final prediction. Given the huge decrease in performance (see Fig. 5), we conclude that cross-entropy is a good alternative to 3D losses used in all prior works such as [7, 19, 25, 36, 73]. The use of the PVE produces sequences of indices corresponding to anthropomorphic results.

“No reprojection” means that we do not compute the reprojection error. This mostly increases the error in PVE and MPJPE, which was expected since the PA-MPJPE is only related to the canonical mesh, and the reprojection loss is not used to train the canonical mesh predictor. However, it still has an impact since the canonical mesh prediction is conditioned on the predicted rotation.

In “Mesh-VQ-VAE”, we train Mesh-VQ-VAE only on the AMASS [43] dataset instead of using 3DPW for finetuning as explained in Sec. 4.2. This highlights the importance of this core component in our approach. As Mesh-VQ-VAE is frozen during the VQ-HPS training (see Sec. 4.2), it is crucial to have a good model, and this could be one of the major areas for improvement in our approach.

¹These are results obtained on the valid test set of 3DPW, which is the standard practice [7, 25, 36]. Evaluating on the full 3DPW test set would give a PVE of 184.08 mm, an MPJPE of 157.49 mm, and a PA-MPJPE of 87.12 mm

²These are results obtained on the valid test set of 3DPW, which is the standard practice [7, 25, 36]. Evaluating on the full 3DPW test set would give a PVE of 180.31 mm, an MPJPE of 153.20 mm, and a PA-MPJPE of 87.12 mm

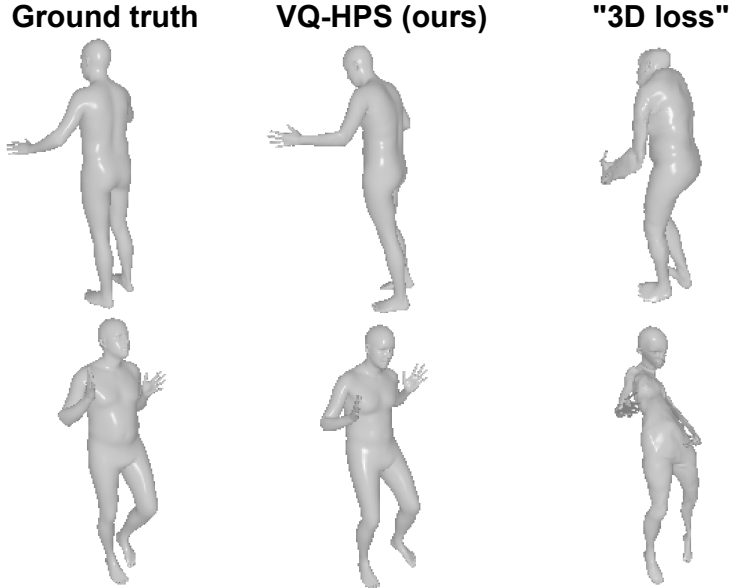


Figure 5: **Ablation study.** Effect of the “3D loss” ablation. We can see that replacing the cross-entropy with a PVE loss produces unnatural poses, showing the interest of our classification-based approach.

Method	PVE ↓	MPJPE ↓	PA-MPJPE ↓
VQ-HPS	184.08	157.49	87.12
3D loss	233.81	210.41	148.08
No reprojection	193.34	167.00	90.46
Mesh-VQ-VAE	192.32	165.50	91.90

Table 2: **Ablation study.** We perform several ablations on the VQ-HPS architecture and training process.

6 Conclusion

In this work, we proposed Mesh-VQ-VAE, an autoencoder architecture providing a discrete latent representation of registered human meshes. This discrete representation allowed us to tackle the HPSE problem from a classification perspective. It allowed us to avoid the limitations of parametric and non-parametric HPSE methods described in Sec. 1. We also introduced VQ-HPS, a transformer-based model for solving the proposed HPSE classification problem. While being trained using the cross-entropy loss, VQ-HPS outperforms state-of-the-art methods on the 3DPW benchmark, showing the potential of the classification approach for human pose and shape estimation.

Limitations and future works. Despite showing great performance when trained on the 3DPW training set, further experiments would need to be performed with VQ-HPS in order to show its superiority over state-of-the-art methods. We believe that the next step will be to train VQ-HPS on more data. However, a constraint for training our model is the need for 3D mesh ground truth. A potential solution for this problem would be the use of synthetic datasets such as [3, 47]. The evaluation may also be performed on other datasets such as [23, 27].

Failure cases are shown in Fig. 6. We believe that working on videos would solve the problem of occlusions and global orientation. The use of bigger backbones such as [66] pre-trained on pose estimation task would also improve the results and might be sufficient to solve the poor results in the case of bad lighting. Finally, improving the Mesh-VQ-VAE model would probably allow us to avoid unrealistic features such as non-anthropomorphic hands (see the first prediction of Fig. 6).



Figure 6: **Failure cases.** VQ-HPS struggles in certain conditions. It sometimes predicts a mesh rotated by 180 degrees relative to the ground truth, especially for symmetric poses. It can also produce wrong predictions when lighting conditions or visibility are bad.

References

- [1] D. Anguelov, P. Srinivasan, D. Koller, S. Thrun, J. Rodgers, and J. Davis. Scape: Shape completion and animation of people. *ACM Transactions on Graphics (TOG)*, 24(3), 2005.
- [2] B. Biggs, D. Novotny, S. Ehrhardt, H. Joo, B. Graham, and A. Vedaldi. 3d multi-bodies: Fitting sets of plausible 3d human models to ambiguous image data. *Advances in Neural Information Processing Systems (NIPS)*, 33:20496–20507, 2020.
- [3] M. J. Black, P. Patel, J. Tesch, and J. Yang. BEDLAM: A synthetic dataset of bodies exhibiting detailed lifelike animated motion. In *IEEE/CVF Conference on Computer Vision and Pattern Recognition (CVPR)*, pages 8726–8737, 2023.
- [4] F. Bogo, A. Kanazawa, C. Lassner, P. Gehler, J. Romero, and M. J. Black. Keep it SMPL: Automatic estimation of 3D human pose and shape from a single image. In *European Conference on Computer Vision (ECCV)*, pages 561–578. Springer, 2016.
- [5] Z. Cai, W. Yin, A. Zeng, C. Wei, Q. Sun, Y. Wang, H. E. Pang, H. Mei, M. Zhang, L. Zhang, et al. Smpler-x: Scaling up expressive human pose and shape estimation. *Advances in Neural Information Processing Systems (NIPS)*, 36, 2023.
- [6] Z. Cai, M. Zhang, J. Ren, C. Wei, D. Ren, Z. Lin, H. Zhao, L. Yang, and Z. Liu. Playing for 3d human recovery. *arXiv preprint arXiv:2110.07588*, 2021.

- [7] J. Cho, K. Youwang, and T.-H. Oh. Cross-attention of disentangled modalities for 3d human mesh recovery with transformers. In *European Conference on Computer Vision (ECCV)*, pages 342–359. Springer, 2022.
- [8] H. Choi, G. Moon, J. Y. Chang, and K. M. Lee. Beyond static features for temporally consistent 3d human pose and shape from a video. In *IEEE/CVF Conference on Computer Vision and Pattern Recognition (CVPR)*, pages 1964–1973, 2021.
- [9] H. Choi, G. Moon, and K. M. Lee. Pose2mesh: Graph convolutional network for 3d human pose and mesh recovery from a 2d human pose. In *European Conference on Computer Vision (ECCV)*, pages 769–787. Springer, 2020.
- [10] N. Cihan Camgoz, S. Hadfield, O. Koller, and R. Bowden. Subunets: End-to-end hand shape and continuous sign language recognition. In *IEEE/CVF International Conference on Computer Vision (ICCV)*, pages 3056–3065, 2017.
- [11] I. Cohen and H. Li. Inference of human postures by classification of 3d human body shape. In *IEEE International Workshop on Analysis and Modeling of Faces and Gestures*, pages 74–81, 2003.
- [12] E. Corona, G. Pons-Moll, G. Alenyà, and F. Moreno-Noguer. Learned vertex descent: a new direction for 3d human model fitting. In *European Conference on Computer Vision (ECCV)*, pages 146–165. Springer, 2022.
- [13] A. Dosovitskiy, L. Beyer, A. Kolesnikov, D. Weissenborn, X. Zhai, T. Unterthiner, M. Dehghani, M. Minderer, G. Heigold, S. Gelly, J. Uszkoreit, and N. Houlsby. An image is worth 16x16 words: Transformers for image recognition at scale. In *International Conference on Learning Representations (ICLR)*, 2021.
- [14] Z. Dou, Q. Wu, C. Lin, Z. Cao, Q. Wu, W. Wan, T. Komura, and W. Wang. Tore: Token reduction for efficient human mesh recovery with transformer. In *IEEE/CVF International Conference on Computer Vision (ICCV)*, pages 15143–15155, 2023.
- [15] M. Einfalt, D. Zecha, and R. Lienhart. Activity-conditioned continuous human pose estimation for performance analysis of athletes using the example of swimming. In *IEEE/CVF Winter conference on Applications of Computer Vision (WACV)*, pages 446–455. IEEE, 2018.
- [16] T. Fan, K. V. Alwala, D. Xiang, W. Xu, T. Murphey, and M. Mukadam. Revitalizing optimization for 3d human pose and shape estimation: A sparse constrained formulation. In *IEEE/CVF International Conference on Computer Vision (ICCV)*, pages 11457–11466, 2021.
- [17] Q. Fang, K. Chen, Y. Fan, Q. Shuai, J. Li, and W. Zhang. Learning analytical posterior probability for human mesh recovery. In *IEEE/CVF Conference on Computer Vision and Pattern Recognition (CVPR)*, pages 8781–8791, 2023.
- [18] A. Feng, S. Shin, and Y. Yoon. A tool for extracting 3d avatar-ready gesture animations from monocular videos. In *ACM SIGGRAPH Conference on Motion, Interaction and Games (ACM MIG)*, pages 1–7, 2022.
- [19] S. Goel, G. Pavlakos, J. Rajasegaran, A. Kanazawa, and J. Malik. Humans in 4d: Reconstructing and tracking humans with transformers. In *IEEE/CVF International Conference on Computer Vision (ICCV)*, pages 14783–14794, 2023.
- [20] R. A. Guler and I. Kokkinos. Holopose: Holistic 3d human reconstruction in-the-wild. In *IEEE/CVF Conference on Computer Vision and Pattern Recognition (CVPR)*, pages 10884–10894, 2019.
- [21] G. Guo, Y. Fu, C. R. Dyer, and T. S. Huang. Head pose estimation: Classification or regression? In *International Conference on Pattern Recognition (ICPR)*, pages 1–4. IEEE, 2008.
- [22] K. He, X. Zhang, S. Ren, and J. Sun. Deep residual learning for image recognition. In *IEEE/CVF Conference on Computer Vision and Pattern Recognition (CVPR)*, pages 770–778, 2016.
- [23] C. Ionescu, D. Papava, V. Olaru, and C. Sminchisescu. Human3.6m: Large scale datasets and predictive methods for 3d human sensing in natural environments. *IEEE Transactions on Pattern Analysis and Machine Intelligence (PAMI)*, 36(7):1325–1339, 2013.
- [24] H. Joo, N. Neverova, and A. Vedaldi. Exemplar fine-tuning for 3d human model fitting towards in-the-wild 3d human pose estimation. In *International Conference on 3D Vision (3DV)*, pages 42–52. IEEE, 2021.
- [25] A. Kanazawa, M. J. Black, D. W. Jacobs, and J. Malik. End-to-end recovery of human shape and pose. In *IEEE/CVF Conference on Computer Vision and Pattern Recognition (CVPR)*, pages 7122–7131, 2018.
- [26] A. Kanazawa, J. Y. Zhang, P. Felsen, and J. Malik. Learning 3d human dynamics from video. In *IEEE/CVF Conference on Computer Vision and Pattern Recognition (CVPR)*, pages 5614–5623, 2019.
- [27] M. Kaufmann, J. Song, C. Guo, K. Shen, T. Jiang, C. Tang, J. J. Zárate, and O. Hilliges. EMDB: The Electromagnetic Database of Global 3D Human Pose and Shape in the Wild. In *IEEE/CVF International Conference on Computer Vision (ICCV)*, pages 14632–14643, 2023.

- [28] C. Keskin, F. Kırac, Y. E. Kara, and L. Akarun. Hand pose estimation and hand shape classification using multi-layered randomized decision forests. In *European Conference on Computer Vision (ECCV)*, pages 852–863. Springer, 2012.
- [29] M. Kocabas, N. Athanasiou, and M. J. Black. Vibe: Video inference for human body pose and shape estimation. In *IEEE/CVF Conference on Computer Vision and Pattern Recognition (CVPR)*, pages 5253–5263, 2020.
- [30] M. Kocabas, C.-H. P. Huang, O. Hilliges, and M. J. Black. PARE: Part attention regressor for 3D human body estimation. In *IEEE/CVF International Conference on Computer Vision (ICCV)*, pages 11127–11137, 2021.
- [31] N. Kolotouros, G. Pavlakos, M. J. Black, and K. Daniilidis. Learning to reconstruct 3d human pose and shape via model-fitting in the loop. In *IEEE/CVF International Conference on Computer Vision (ICCV)*, pages 2252–2261, 2019.
- [32] N. Kolotouros, G. Pavlakos, and K. Daniilidis. Convolutional mesh regression for single-image human shape reconstruction. In *IEEE/CVF Conference on Computer Vision and Pattern Recognition (CVPR)*, pages 4501–4510, 2019.
- [33] N. Kolotouros, G. Pavlakos, D. Jayaraman, and K. Daniilidis. Probabilistic modeling for human mesh recovery. In *IEEE/CVF Conference on Computer Vision and Pattern Recognition (CVPR)*, pages 11605–11614, 2021.
- [34] C. Lassner, J. Romero, M. Kiefel, F. Bogo, M. J. Black, and P. V. Gehler. Unite the people: Closing the loop between 3d and 2d human representations. In *IEEE/CVF Conference on Computer Vision and Pattern Recognition (CVPR)*, pages 6050–6059, 2017.
- [35] Y. Li, S. Yang, P. Liu, S. Zhang, Y. Wang, Z. Wang, W. Yang, and S.-T. Xia. Simcc: A simple coordinate classification perspective for human pose estimation. In *European Conference on Computer Vision (ECCV)*, pages 89–106. Springer, 2022.
- [36] Z. Li, J. Liu, Z. Zhang, S. Xu, and Y. Yan. Cliff: Carrying location information in full frames into human pose and shape estimation. In *European Conference on Computer Vision (ECCV)*, pages 590–606. Springer, 2022.
- [37] J. Lin, A. Zeng, H. Wang, L. Zhang, and Y. Li. One-stage 3d whole-body mesh recovery with component aware transformer. In *IEEE/CVF Conference on Computer Vision and Pattern Recognition (CVPR)*, pages 21159–21168, 2023.
- [38] K. Lin, L. Wang, and Z. Liu. End-to-end human pose and mesh reconstruction with transformers. In *IEEE/CVF Conference on Computer Vision and Pattern Recognition (CVPR)*, pages 1954–1963, 2021.
- [39] K. Lin, L. Wang, and Z. Liu. Mesh graphormer. In *IEEE/CVF International Conference on Computer Vision (ICCV)*, pages 12939–12948, 2021.
- [40] M. Loper, N. Mahmood, J. Romero, G. Pons-Moll, and M. J. Black. Smpl: A skinned multi-person linear model. *ACM Transactions on Graphics (TOG)*, 34(6), 2015.
- [41] T. Lucas, F. Baradel, P. Weinzaepfel, and G. Rogez. Posegpt: Quantization-based 3d human motion generation and forecasting. In *European Conference on Computer Vision (ECCV)*, pages 417–435. Springer, 2022.
- [42] Z. Luo, S. A. Golestaneh, and K. M. Kitani. 3d human motion estimation via motion compression and refinement. In *Asian Conference on Computer Vision (ACCV)*, 2020.
- [43] N. Mahmood, N. Ghorbani, N. F. Troje, G. Pons-Moll, and M. J. Black. Amass: Archive of motion capture as surface shapes. In *IEEE/CVF International Conference on Computer Vision (ICCV)*, pages 5442–5451, 2019.
- [44] G. Moon, H. Choi, and K. M. Lee. Neuralannot: Neural annotator for 3d human mesh training sets. In *IEEE/CVF Conference on Computer Vision and Pattern Recognition (CVPR)*, pages 2299–2307, 2022.
- [45] G. Moon and K. M. Lee. I2l-meshnet: Image-to-lixel prediction network for accurate 3d human pose and mesh estimation from a single rgb image. In *European Conference on Computer Vision (ECCV)*, pages 752–768. Springer, 2020.
- [46] A. A. A. Osman, T. Bolkart, D. Tzionas, and M. J. Black. SUPR: A sparse unified part-based human representation. In *European Conference on Computer Vision (ECCV)*, pages 568–585. Springer, 2022.
- [47] P. Patel, C.-H. P. Huang, J. Tesch, D. T. Hoffmann, S. Tripathi, and M. J. Black. AGORA: Avatars in geography optimized for regression analysis. In *IEEE/CVF Conference on Computer Vision and Pattern Recognition (CVPR)*, pages 13468–13478, 2021.
- [48] G. Pavlakos, V. Choutas, N. Ghorbani, T. Bolkart, A. A. A. Osman, D. Tzionas, and M. J. Black. Expressive body capture: 3d hands, face, and body from a single image. In *IEEE/CVF Conference on Computer Vision and Pattern Recognition (CVPR)*, pages 10975–10985, 2019.

- [49] D. Rempe, T. Birdal, A. Hertzmann, J. Yang, S. Sridhar, and L. J. Guibas. Humor: 3d human motion model for robust pose estimation. In *IEEE/CVF International Conference on Computer Vision (ICCV)*, pages 11488–11499, 2021.
- [50] G. Rogez and C. Schmid. Mocap-guided data augmentation for 3d pose estimation in the wild. *Advances in neural information processing systems (NIPS)*, 29:3108–3116, 2016.
- [51] G. Rogez, P. Weinzaepfel, and C. Schmid. Lcr-net++: Multi-person 2d and 3d pose detection in natural images. *IEEE Transactions on Pattern Analysis and Machine Intelligence (PAMI)*, 42(5):1146–1161, 2019.
- [52] O. Russakovsky, J. Deng, H. Su, J. Krause, S. Satheesh, S. Ma, Z. Huang, A. Karpathy, A. Khosla, M. Bernstein, et al. Imagenet large scale visual recognition challenge. *International Journal of Computer Vision (IJCV)*, 115:211–252, 2015.
- [53] P. Sarakon, T. Charoenpong, and S. Charoensiriwath. Face shape classification from 3d human data by using svm. In *Biomedical Engineering International Conference*, pages 1–5. IEEE, 2014.
- [54] A. Sengupta, I. Budvytis, and R. Cipolla. Probabilistic 3d human shape and pose estimation from multiple unconstrained images in the wild. In *IEEE/CVF Conference on Computer Vision and Pattern Recognition (CVPR)*, pages 16094–16104, 2021.
- [55] A. Sengupta, I. Budvytis, and R. Cipolla. Humaniflow: Ancestor-conditioned normalising flows on so (3) manifolds for human pose and shape distribution estimation. In *IEEE/CVF Conference on Computer Vision and Pattern Recognition (CVPR)*, pages 4779–4789, 2023.
- [56] M. Shi, S. Starke, Y. Ye, T. Komura, and J. Won. Phasemp: Robust 3d pose estimation via phase-conditioned human motion prior. In *IEEE/CVF International Conference on Computer Vision (ICCV)*, pages 14725–14737, 2023.
- [57] L. Siyao, W. Yu, T. Gu, C. Lin, Q. Wang, C. Qian, C. C. Loy, and Z. Liu. Bailando: 3d dance generation by actor-critic gpt with choreographic memory. In *IEEE/CVF Conference on Computer Vision and Pattern Recognition (CVPR)*, pages 11050–11059, 2022.
- [58] S. Starke, I. Mason, and T. Komura. Deepphase: Periodic autoencoders for learning motion phase manifolds. *ACM Transactions on Graphics (TOG)*, 41(4), 2022.
- [59] G. Tiwari, D. Antic, J. E. Lenssen, N. Sarafianos, T. Tung, and G. Pons-Moll. Pose-ndf: Modeling human pose manifolds with neural distance fields. In *European Conference on Computer Vision (ECCV)*, pages 572–589. Springer, 2022.
- [60] A. Van Den Oord, O. Vinyals, et al. Neural discrete representation learning. *Advances in neural information processing systems (NIPS)*, 30:6306–6315, 2017.
- [61] G. Varol, J. Romero, X. Martin, N. Mahmood, M. J. Black, I. Laptev, and C. Schmid. Learning from synthetic humans. In *IEEE/CVF Conference on Computer Vision and Pattern Recognition (CVPR)*, pages 109–117, 2017.
- [62] A. Vaswani, N. Shazeer, N. Parmar, J. Uszkoreit, L. Jones, A. N. Gomez, Ł. Kaiser, and I. Polosukhin. Attention is all you need. *Advances in Neural Information Processing Systems (NIPS)*, 30:5998–6008, 2017.
- [63] T. von Marcard, R. Henschel, M. Black, B. Rosenhahn, and G. Pons-Moll. Recovering accurate 3d human pose in the wild using imus and a moving camera. In *European Conference on Computer Vision (ECCV)*, pages 601–617. Springer, 2018.
- [64] D. Wang and S. Zhang. 3d human mesh recovery with sequentially global rotation estimation. In *IEEE/CVF International Conference on Computer Vision (ICCV)*, pages 14953–14962, 2023.
- [65] J. Wang, K. Qiu, H. Peng, J. Fu, and J. Zhu. Ai coach: Deep human pose estimation and analysis for personalized athletic training assistance. In *ACM International Conference on Multimedia (ACM MM)*, pages 374–382, 2019.
- [66] J. Wang, K. Sun, T. Cheng, B. Jiang, C. Deng, Y. Zhao, D. Liu, Y. Mu, M. Tan, X. Wang, et al. Deep high-resolution representation learning for visual recognition. *IEEE transactions on Pattern Analysis and Machine Intelligence (PAMI)*, 43(10):3349–3364, 2020.
- [67] H. Xu, E. G. Bazavan, A. Zanfir, W. T. Freeman, R. Sukthankar, and C. Sminchisescu. Ghum & ghuml: Generative 3d human shape and articulated pose models. In *IEEE/CVF Conference on Computer Vision and Pattern Recognition (CVPR)*, pages 6184–6193, 2020.
- [68] X. Xu, H. Chen, F. Moreno-Noguer, L. A. Jeni, and F. De la Torre. 3d human shape and pose from a single low-resolution image with self-supervised learning. In *European Conference on Computer Vision (ECCV)*, pages 284–300. Springer, 2020.

- [69] X. Xu, H. Chen, F. Moreno-Noguer, L. A. Jeni, and F. De la Torre. 3d human pose, shape and texture from low-resolution images and videos. *IEEE Transactions on Pattern Analysis and Machine Intelligence (PAMI)*, 44(9):4490–4504, 2021.
- [70] S. Yang, Z. Wu, M. Li, Z. Zhang, L. Hao, W. Bao, and H. Zhuang. Qpgesture: Quantization-based and phase-guided motion matching for natural speech-driven gesture generation. In *IEEE/CVF Conference on Computer Vision and Pattern Recognition (CVPR)*, pages 2321–2330, 2023.
- [71] A. Zanfır, E. Marinoiu, and C. Sminchisescu. Monocular 3d pose and shape estimation of multiple people in natural scenes-the importance of multiple scene constraints. In *IEEE/CVF Conference on Computer Vision and Pattern Recognition (CVPR)*, pages 2148–2157, 2018.
- [72] H. Zhang, J. Cao, G. Lu, W. Ouyang, and Z. Sun. Learning 3d human shape and pose from dense body parts. *IEEE Transactions on Pattern Analysis and Machine Intelligence (PAMI)*, 44(5):2610–2627, 2020.
- [73] H. Zhang, Y. Tian, X. Zhou, W. Ouyang, Y. Liu, L. Wang, and Z. Sun. Pymaf: 3d human pose and shape regression with pyramidal mesh alignment feedback loop. In *IEEE/CVF International Conference on Computer Vision (ICCV)*, pages 11446–11456, 2021.
- [74] H. Zhang, Y. Yuan, V. Makoviychuk, Y. Guo, S. Fidler, X. B. Peng, and K. Fatahalian. Learning physically simulated tennis skills from broadcast videos. *ACM Transactions on Graphics (TOG)*, 42(4), 2023.
- [75] J. Zhang, Y. Zhang, X. Cun, S. Huang, Y. Zhang, H. Zhao, H. Lu, and X. Shen. T2m-gpt: Generating human motion from textual descriptions with discrete representations. *arXiv preprint arXiv:2301.06052*, 2023.
- [76] C. Zheng, X. Liu, G.-J. Qi, and C. Chen. Potter: Pooling attention transformer for efficient human mesh recovery. In *IEEE/CVF Conference on Computer Vision and Pattern Recognition (CVPR)*, pages 1611–1620, 2023.
- [77] Y. Zhou, C. Barnes, J. Lu, J. Yang, and H. Li. On the continuity of rotation representations in neural networks. In *IEEE/CVF Conference on Computer Vision and Pattern Recognition (CVPR)*, pages 5745–5753, 2019.
- [78] Y. Zhou, C. Wu, Z. Li, C. Cao, Y. Ye, J. Saragih, H. Li, and Y. Sheikh. Fully convolutional mesh autoencoder using efficient spatially varying kernels. *Advances in neural information processing systems (NIPS)*, 33:9251–9262, 2020.